Insight into the electronic structure of semiconducting ϵ-GaSe and ϵ-InSe

S. V. Eremeev,[1,2,3] M. Papagno,[4] I. Grimaldi,[4] O. De Luca,[4] L. Ferrari,[5] Asish K. Kundu,[6] P. M. Sheverdyaeva,[6] P. Moras,[6] G. Avvisati,[7] A. Crepaldi,[8] H. Berger,[8] I. Vobornik,[9] M. G. Betti,[7] M. Grioni,[8] C. Carbone,[6] E. V. Chulkov,[3,10,11] and D. Pacilé[4,*]

[1]*Institute of Strength Physics and Materials Science, 634055 Tomsk, Russia*
[2]*Tomsk State University, 634050 Tomsk, Russia*
[3]*Saint Petersburg State University, Laboratory of Electronic and Spin Structure of Nanosystems, 198504 Saint Petersburg, Russia*
[4]*Dipartimento di Fisica, Università della Calabria, 87036 Arcavacata di Rende (CS), Italy*
[5]*Istituto di Struttura della Materia, Consiglio Nazionale delle Ricerche, Roma, Italy*
[6]*Istituto di Struttura della Materia, Consiglio Nazionale delle Ricerche, Trieste, Italy*
[7]*Dipartimento di Fisica, Università di Roma "La Sapienza," I-00185 Roma, Italy*
[8]*Insitute of Physics, Ecole Polytechnique Fédérale de Lausanne (EPFL), CH-1015 Lausanne, Switzerland*
[9]*Istituto Officina dei Materiali (IOM)-CNR, Laboratorio TASC, Area Science Park, S.S.14, Km 163.5, 34149 Trieste, Italy*
[10]*Donostia International Physics Center, 20018 Donostia–San Sebastian, Basque Country, Spain*
[11]*Departamento de Fisica de Materiales UPV/EHU, Centro de Fisica de Materiales CFM MPC, and Centro Mixto CSICUPV/EHU, 20080 Donostia–San Sebastian, Basque Country, Spain*

(Received 1 May 2020; accepted 5 August 2020; published 26 August 2020)

Metal monochalcogenides (MX) have recently been rediscovered as two-dimensional materials with electronic properties highly dependent on the number of layers. Although some intriguing properties appear in the few-layer regime, the carrier mobility of MX compounds increases with the number of layers, motivating the interest in multilayered heterostructures or bulk materials. By means of angle-resolved photoemission spectroscopy (ARPES) measurements and density functional theory calculations, we compare the electronic band structure of bulk ϵ-GaSe and ϵ-InSe semiconductors. We focus our attention on the top valence band of the two compounds along main symmetry directions, discussing the effect of spin-orbit coupling and contributions from post-transition-metal (Ga or In) and Se atoms. Our results show that the top valence band at Γ point is dominated by Se p_z states, while the main effect of Ga or In appears more deeply in binding energy, at the Brillouin zone corners, and in the conduction band. These findings explain also the experimental observation of a hole effective mass rather insensitive to the post-transition metal. Finally, by means of spin-resolved ARPES and surface band structure calculations we describe Rashba-Bychkov spin splitting of surface states in ϵ-InSe.

DOI: 10.1103/PhysRevMaterials.4.084603

I. INTRODUCTION

The electronic properties of layered monochalcogenides (MX, where M stands for the post-transition metal, and X represents the chalcogen atom), among them GaSe and InSe, have recently been the focus of extensive research, mainly devoted to the discovery of unique properties in the few-layers regime [1–6]. MX compounds exhibit a direct band gap in the bulk [GaSe of about 2.0 eV [7] and InSe of about 1.3 eV [8] at room temperature (RT)], while they acquire an indirect band gap for few layers. Films of different thickness exhibit variable width of the band gap, thus they are optically active in the IR and visible region and are tested as active components in photodetectors [3,9,10]. Moreover, vertical van der Waals (vdW) heterostructures obtained by combining different two-dimensional (2D) materials have been investigated in order to create novel functionalities [11–15], or to increase the carrier mobility [8,16].

The possibility to manipulate vertical vdW heterostructures requires detailed knowledge of single components, starting from the bulk counterpart down to a single layer. Through angle-resolved photoemission spectroscopy (ARPES) measurements and density functional theory (DFT) calculations, the present study aims at clarifying the role of the metal and Se chalcogenide atoms in the bulk electronic structure of two related MX compounds, ϵ-GaSe and ϵ-InSe. The single tetralayer of each compound consists of four covalently bonded Se-M-M-Se atoms (M stands for Ga or In), while different tetralayers are held together by vdW forces, making the compounds easily exfoliable. For each MX compound there are different polytypes (ϵ-MSe, β-MSe, γ-MSe, δ-MSe) [17,18], which differ in the symmetry and structure of the crystal lattice, and present specific physical properties [19]. The bulk ϵ polytype [Fig. 1(a)] is made up by superposition of a pair of tetralayers with AB stacking. It belongs to the $P\bar{6}/m2$ noncentrosymmetric space group (D^1_{3h}), regardless of the number of layers.

It has been widely shown that both ϵ-GaSe and ϵ-InSe have band edges located at Γ in the bulk structure [11,12], while

*daniela.pacile@fis.unical.it

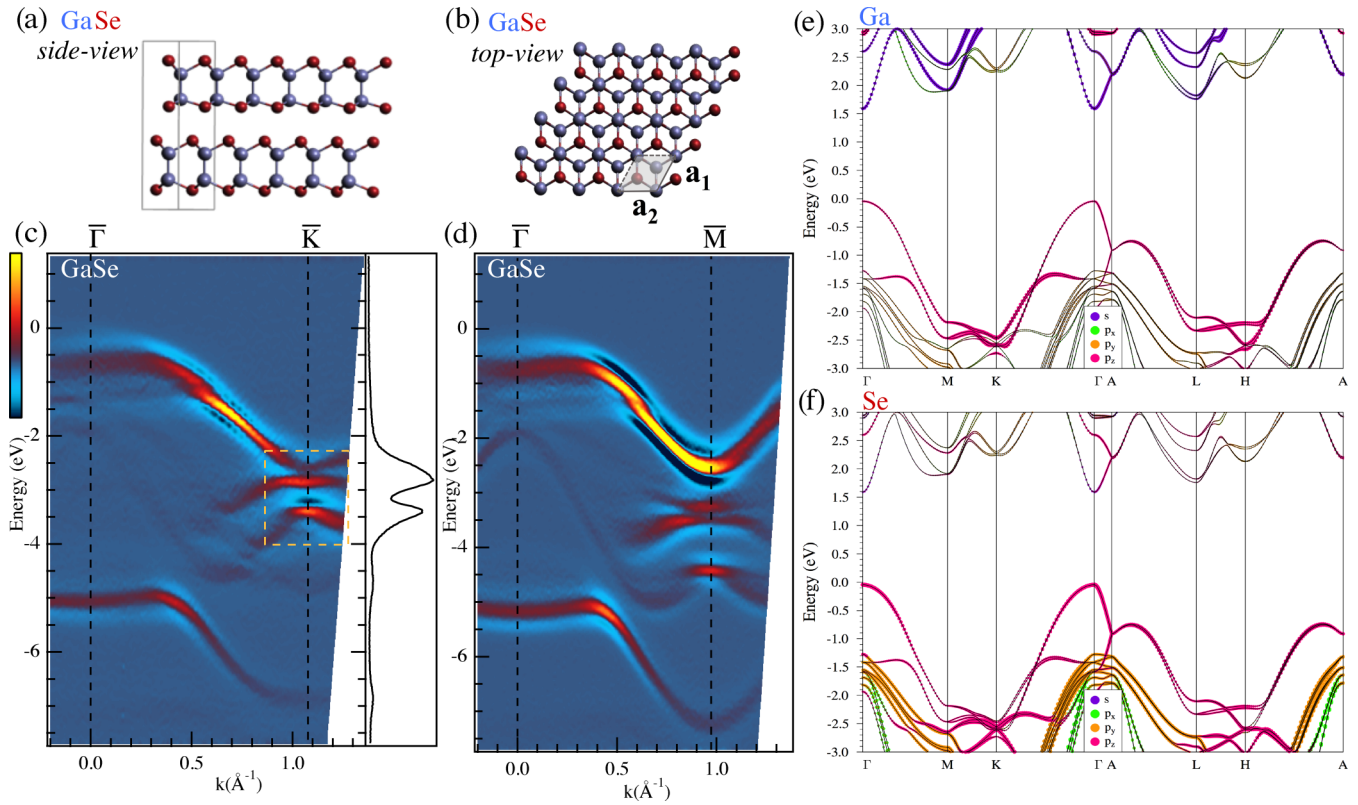

FIG. 1. Sketch of the ϵ-GaSe crystal structure: (a) side view; (b) top view. Experimental band structure, shown in second derivative, along $\bar{\Gamma}$-$\bar{K}$ (c) and $\bar{\Gamma}$-$\bar{M}$ (d), taken with photon energy of 45 eV. On the right side of panel (c), the energy distribution curve extracted from raw data at the $\bar{K}$ point is reported. (e), (f) Calculated orbital-projected bulk band structure along high-symmetry directions of hexagonal Brillouin zone with weights of Ga (e) and Se (f) orbitals, where sizes of the circles are proportional to the contribution of the corresponding orbitals.

decreasing the number of layers the valence band maximum (VBM) slightly shifts away from Γ, creating a bow-shaped valence band, often called inverted "Mexican hat" [20]. The band structure in the few-layers regime has attracted most of the attention as the peculiar shape yields high density of states and Van Hove singularity near the VBM, leading to unconventional correlation effects [21]. Concerning bulk GaSe and InSe, it has been shown that spin-orbit interaction of *MX* compounds lifts band degeneracies, causing a splitting of several hundreds of meV just below the VBM, and yielding measurable differences in high-energy photoluminescence transition energies [11,12].

Since the first days of discovery of these semiconductors [22], the high carrier mobility and its physical mechanism have been the subject of discussion between different authors [23–25]. The understanding of these properties requires wide-spectrum information on the electronic band structure. Our ARPES and DFT study of ϵ-GaSe and ϵ-InSe sheds light on the atomic contributions to the conduction and valence bands. We show that the post-transition metal has a key role in tuning the energy position of the conduction band minimum (CBM) and the energy width of the band gap, leaving unaffected the shape of the top valence band. Spin-ARPES measurements of ϵ-InSe show Rashba-Bychkov spin splitting of localized surface states. The description of our results has involved a careful comparison with different theoretical approaches.

II. METHODS

Single-crystalline ingots of GaSe and InSe were grown in double-wall ampoules by means of the Bridgman method starting from a nonstoichiometric melt, containing an In excess of about 5% [26]. The high quality of the as-grown ingots, as well as the structural phase (ϵ polytype) of InSe was proved by using x-ray diffraction (XRD), transmission electron microscopy and Raman spectroscopy, and reported elsewhere [27]. The XRD characterization of ϵ-GaSe is instead reported in the Supplemental Material [28–30] (Fig. S1). Photoemission measurements were performed on fresh surfaces obtained by cleavage at RT in UHV conditions. The high quality of the achieved (111) surfaces was verified by sharp features in the low-energy electron diffraction (LEED) pattern, reported in the Supplemental Material [28] (Fig. S2). The ARPES measurements were performed at the VUV photoemission beamline of the Elettra synchrotron, with the sample kept at 18 K, using Scienta R-4000 hemispherical electron analyzer, which allows parallel acquisition over 30° angular range. The energy and angular resolution of ARPES were set to 15 meV and 0.3°, respectively. Spin-resolved ARPES measurements were performed at liquid-nitrogen temperature at the APE beamline of the Elettra synchrotron, by use of a very low-energy electron diffraction–based spin polarimeter [31]. Energy and angular resolution were set to 100 meV and 1.0°.

All ARPES spectra have been aligned to the VBM for an easier comparison with the theoretical band structure and shown as second derivative of the photoemission intensity along the energy axis.

The density functional theory calculations were performed by using the Vienna *Ab initio* Simulation Package (VASP) [32,33], with core electrons represented by projector augmented wave potentials [34,35]. For bulk parameters optimization the generalized gradient approximation (GGA-PBE) [36] to the exchange-correlation potential and DFT-D3 van der Waals correction [37] were applied. The equilibrium lattice parameters of GaSe(InSe) $a = 3.778(4.041)$ Å, $c = 15.943(16.723)$ Å are in fine agreement with experimental data, $a = 3.757(\pm 0.015)$ Å and $c = 15.998(\pm 0.032)$ Å for GaSe, as extracted from Fig. S1, and $a = 4.005(\pm 0.022)$ Å and $c = 16.672(\pm 0.045)$ Å for InSe [27]. However, the bulk gaps obtained within GGA-PBE calculations are much smaller than the experimental values. They are 0.795 eV for GaSe and 0.315 eV for InSe. To obtain more accurate bulk band structures, the modified Becke-Johnson (mBJ) exchange potential [38,39], which has been shown to be the most accurate semilocal potential for band-gap calculations was adopted. The mBJ bulk gaps of 1.801 and 1.087 eV for GaSe and InSe, respectively, are in satisfactory agreement with the experiments. We also have done the calculations using the HSE06 screened hybrid functional [40]. The HSE06 bulk gaps are 1.635 and 1.034 eV for GaSe and InSe, respectively. Spin-orbit interaction was included in all types of calculations.

For surface band structure calculations we use slabs of 56 atomic layers thickness (14 tetralayers) which were relaxed within the GGA-PBE approach with DFT-D3 van der Waals correction included. Atoms of two tetralayers on both sides of the slab were allowed to relax whereas the atoms in the internal layers were fixed to their equilibrium bulk positions.

III. RESULTS AND DISCUSSION

The electronic band structure of ϵ-GaSe and ϵ-InSe was investigated using ARPES and DFT calculations. According to the hexagonal surface symmetry [Fig. 1(b)], an insight in the electronic structure requires the investigation of the band dispersion along two symmetry directions. In Figs. 1(c) and 1(d) we report the GaSe bulk band structure projection on the surface Brillouin zone (BZ) along the $\bar{\Gamma}$-$\bar{K}$ and $\bar{\Gamma}$-$\bar{M}$ directions, taken with photon energy of 45 eV. The topmost part of the valence band is found at the $\bar{\Gamma}$ point, down-dispersing along both high-symmetry directions. In Figs. 1(e) and 1(f) we show the GaSe calculated bands projected on Ga and Se orbitals, respectively. Our simulation proves that for a bulk system the VBM is located at Γ (the bulk Brillouin zone is reported in Fig. S2 of the Supplemental Material [28]), and both systems do have a direct band, in agreement with earlier results [1,4]. By inspection of theoretical results, we prove that the top valence band of bulk GaSe has a dominant p_z component of both Ga and Se atoms [pink circles in Figs. 1(e) and 1(f)], with about two times higher weight of Se atoms. Moreover, below about 1 eV from the VBM, mainly p_y and p_x components of Se atoms [yellow and green circles in Fig. 1(f), respectively] are present. Similar results are obtained for bulk InSe, as reported in Figs. 2(b) and 2(c).

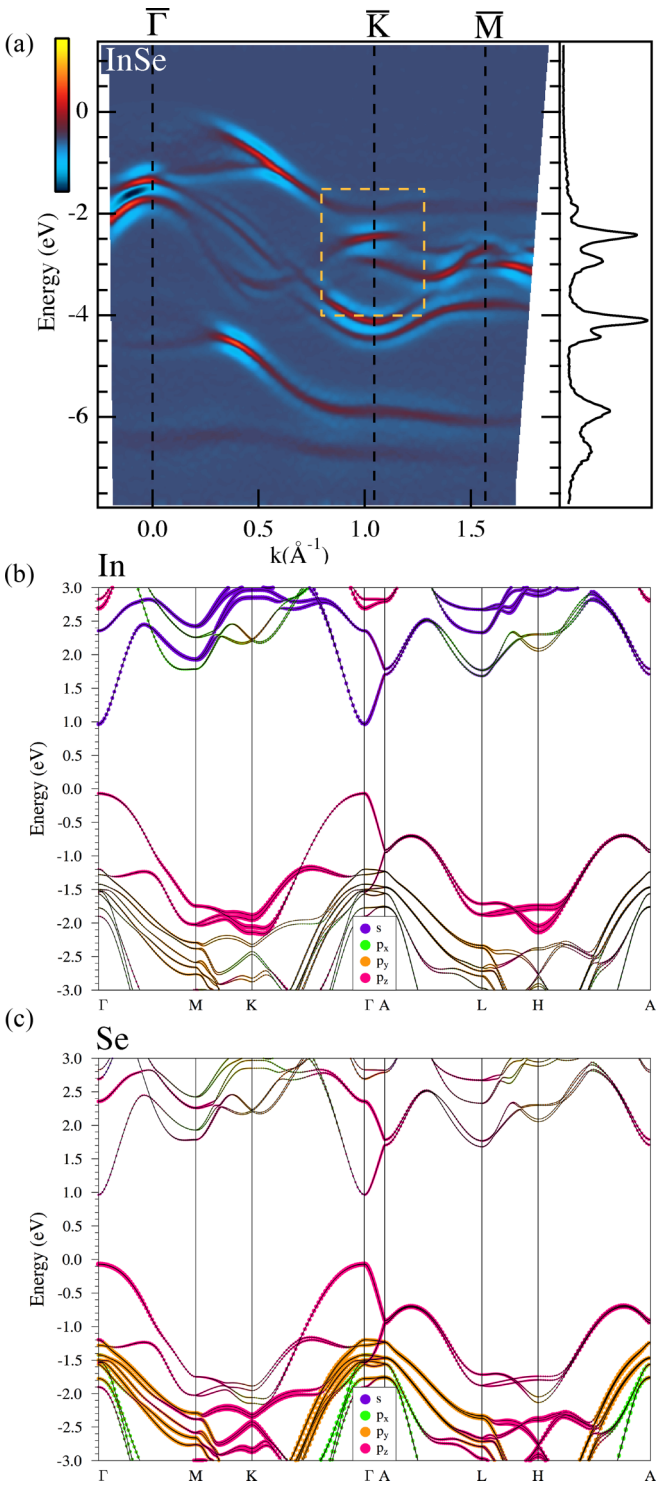

FIG. 2. (a) Experimental band structure of ϵ-InSe, shown in second derivative along $\bar{\Gamma}\bar{K}\bar{M}$, taken with photon energy of 65 eV. On the right side, the energy distribution curve extracted from raw data at the $\bar{K}$ point is reported. (b), (c) The same as in Figs. 1(e) and 1(f) but for In and Se orbitals.

Comparing the two compounds, we deduce that Se p_z states are expected to dominate at the VBM, thus a different group III metal does not change significantly the outer occupied states of the semiconductor. ARPES measurements of ϵ-GaSe

reported in Figs. 1(c) and 1(d) and ϵ-InSe in Fig. 2(a) display similar top valence bands, supporting the theoretical findings. Moreover, the highest bands with a dominant p_z component exhibit a similar slope along the $\bar{\Gamma}$-$\bar{K}$ direction, and reach the $\bar{K}$ point almost flat, due to a reduced and similar length of the c^* reciprocal lattice parameter. Contrarily, lower lying bands with their maximum at about -1.5 eV at the $\bar{\Gamma}$ point, which have dominant p_x and p_y components, as described by our theoretical calculations [yellow and green circles in Figs. 1(f) and 2(c)], exhibit a different slope along $\bar{\Gamma}$-$\bar{K}$. This slope is indeed more pronounced for ϵ-GaSe, which have a slightly higher (of about 7%) a^* reciprocal lattice parameter with respect to ϵ-InSe.

The bottom of the conduction band, instead, is mainly due to Ga (In) s states, thus more sensitive to the post-transition metal. On the other hand, from a closer look at the color scale of the occupied bands in Figs. 1(e) and 1(f) and 2(b) and 2(c), one can see that the p_z weight of Ga/In is prevailing near the corners of the BZ, that is, at the $K(H)$ points. This predicted difference is clearly seen in Figs. 1(c) and 2(a) at the $\bar{K}$ point, as highlighted by dashed yellow lines and energy distribution curves reported on the corresponding right panels. We point out that the two topmost surface projected bands of ϵ-GaSe overlap at the $\bar{K}$ point [Fig. 1(c)], while they are clearly separated by about 0.50 eV for ϵ-InSe [Fig. 2(a)]. The agreement with our simulations along surface symmetry directions, and specifically at the $\bar{K}$ point, is further supported by projected band structure calculations reported in the Supplemental Material [28] (Fig. S3). Here, at the $\bar{K}$ point, the spin-orbit splitting of the topmost band is almost twice larger in InSe (71 meV) as compared to GaSe (40 meV). However, the magnitude of the splitting in both cases is smaller with respect to k_z dispersion of the bands, and this hampers its detection by photoemission.

We further discuss the comparison between the two compounds by focusing on the VBM. In Figs. 3(a) and 3(b) we report the band structure of GaSe and InSe, respectively, along the $\bar{M}$-$\bar{\Gamma}$-$\bar{M}$ high-symmetry axis. We notice that continuum states (highlighted by white arrows) close to the VBM are visible at the selected photon energy for both compounds. From the peak positions of corresponding energy distribution curves, we traced the dispersion of the top valence band [Figs. 3(c) and 3(d)], and estimated the corresponding hole effective mass, obtaining values close to m_e for both compounds. Our findings for InSe are in agreement with previous results extracted at the bulk Γ point with photon energy of 60 eV [12], demonstrating a weak dependence of the effective mass on the wave vector k_z perpendicular to the layers. The comparable hole effective mass of GaSe and InSe provides additional evidence of the dominant Se p_z character of the top valence band.

In order to detect the effect of spin-orbit interaction on the surface electronic structure, we have acquired spin-resolved ARPES measurements for ϵ-InSe (Fig. 4). The measurements were performed at 35 eV of photon energy using linearly p-polarized light. Spin-polarization data were discerned only in the experimental geometry parallel to the plane of incidence. Considering that the APE DA30 momentum dispersion plane is perpendicular to the Elettra orbit, in this geometry the in-plane spin component (along k_y) perpendicular to the selected

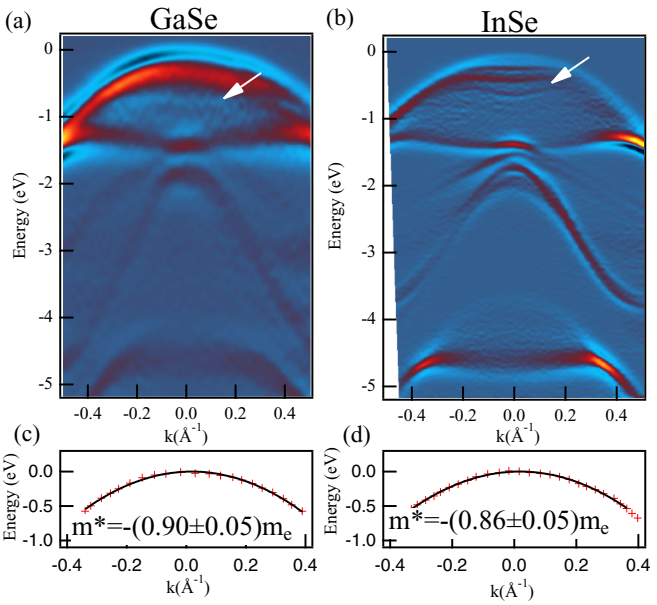

FIG. 3. Experimental band structure of ϵ-GaSe (a) and ϵ-InSe (b), shown in second derivative, taken along the $\bar{M}$-$\bar{\Gamma}$-$\bar{M}$ high-symmetry axis (photon energy is 40 eV). (c), (d) Determination of the hole effective mass through a parabolic model from the experimental dispersion (red crosses) extracted from the top band in (a) and (b), respectively.

high-symmetry direction (along k_x) was probed. Corresponding spin-resolved energy distribution curves, shown at $k_x = (-0.37 \pm 0.05)$ Å^{-1} and $k_x = (0.37 \pm 0.05)$ Å^{-1} (top-left and top-right panels of Fig. 4, respectively) exhibit a considerable spin polarization. Moreover, the spin polarization reverses upon changing the sign of k_x (b, c, and d peaks, located at about 3.6, 3.4, and 3.2 eV from the VBM, respectively) and it vanishes at $k_x = 0$ (data not shown). This observed Rashba-Bychkov-type spin polarization has been explored by means of surface band structure calculations.

First, we compared the valence band calculated within GGA-PBE, HSE06, and mBJ approaches with an experimental spectrum. Despite its failure to reproduce the band gap, GGA-PBE better describes the experimental valence band compared to the other two. The total width of the measured VB at the $\bar{\Gamma}$ point amounts to about 4.5 eV (Fig. 4, center panel). In particular, as can be seen in Fig. 5(a), the deep band, which is mainly composed by In s orbitals hybridized with p_z Se orbitals, is very sensitive to the exchange—correlation functional. The GGA-PBE nicely reproduces the experimental VB width whereas HSE06 (mBJ) noticeably overestimates (underestimates) it. The same behavior is observed for GaSe. For this reason we have done surface band structure calculations within the GGA-PBE approach. Figure 5(b) shows the surface spectrum of InSe. The calculation without spin-orbit coupling (SOC) included (see Fig. S4 of the Supplemental Material [28]) shows that the fundamental band gap in InSe is free of surface states; however, the valence band hosts several localized states, which only slightly split off the edges of the bulk bands. Such appearance of the surface states is typical for layered van der Waals materials where there are no dangling bonds on the cleavage surface and, therefore,

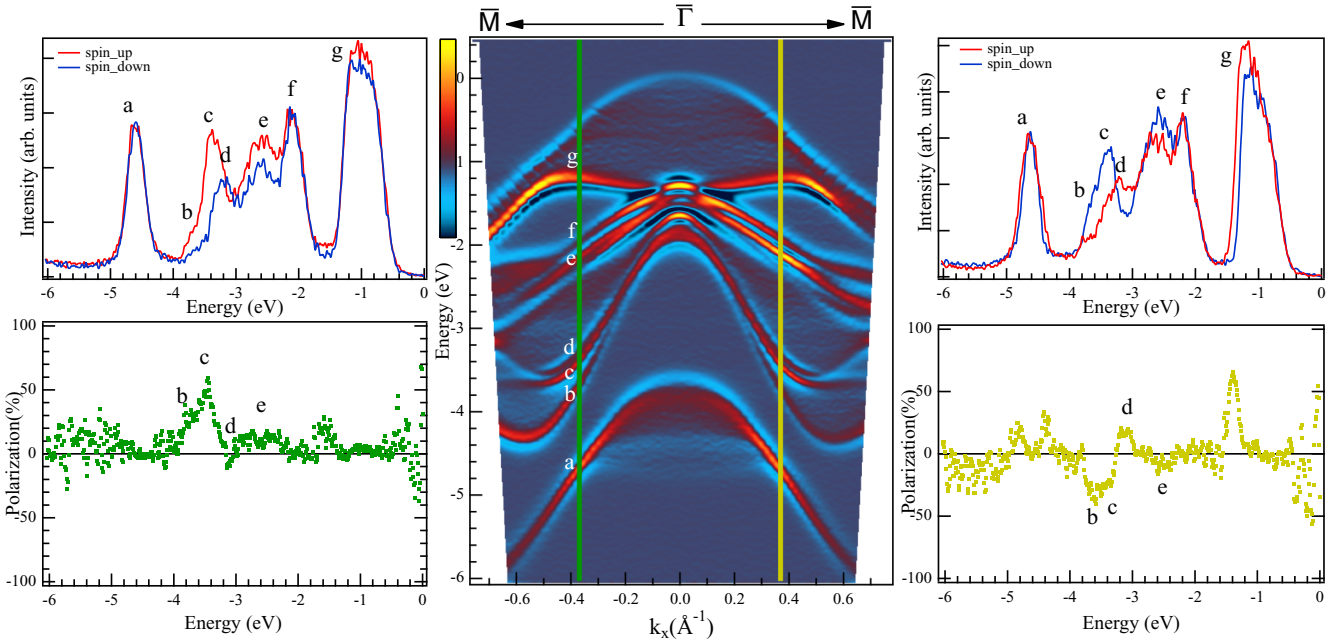

FIG. 4. Spin-ARPES data of ϵ-InSe. Central panel: experimental band structure shown in second derivative along the $\bar{M}$-$\bar{\Gamma}$-$\bar{M}$ high-symmetry axis (photon energy is 35 eV using linearly p-polarized light). Original data are reported in the Supplemental Material [28] (Fig. S2). Left-right panels: spin-resolved curves and corresponding spin polarization showing the spin texture of selected bands indicated by green and yellow lines in the central panel.

the surface potential bending is insignificant. When the SOC is switched on, these surface states acquire the Rashba spin splitting, as follows from the calculated helical spin texture in Fig. 5(b). However, this splitting in general is negligible [red and blue circles in Fig. 5(b) are noticeably overlapped] with the exception of several states which are split off from the edge of the bulk states more than others. For instance, the state located inside the local VB gap which crosses experimental k_x green/yellow lines at about -2.7 eV and whose spin counterpart merges with bulk states, can be confidently identified with the highly spin-polarized experimental peak c even if about 0.6 eV higher in energy. As for other experimental peaks which demonstrate significantly weaker spin polarization or do not show it at all, the corresponding slightly split bands

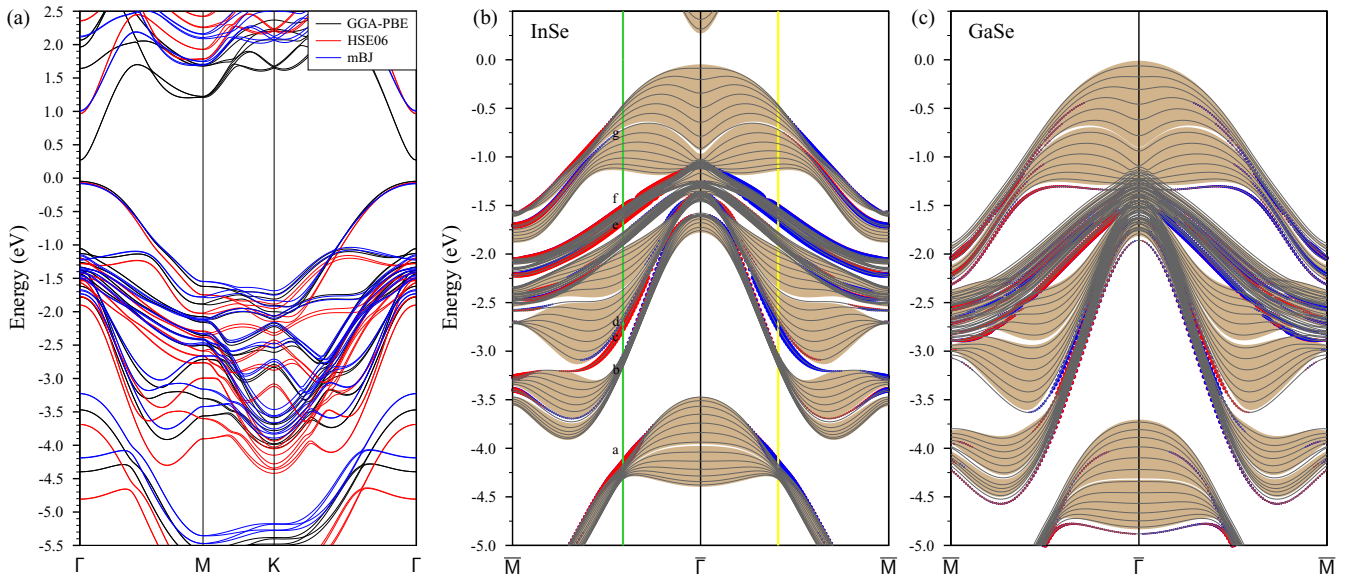

FIG. 5. Bulk band structure of InSe as calculated within GGA-PBE, HSE06, and mBJ approaches (a). Calculated surface electronic structure and spin polarization of InSe (b) and GaSe (c). Red (blue) circles represent positive (negative) sign of the in-plane spin component for the surface states. Shaded areas correspond to projection of the bulk states on the (111) plane. Green and yellow vertical lines in panel (a) mark $k_\parallel$ where the spin polarization was measured; see Fig. 4 (central panel).

can also be found in the calculated spectrum at energies of about 0.5–0.8 eV higher compared to experimental values. The variable difference between calculated and experimental energies is due to a reduced split off between surface states and bulk bands, which would require similar accuracy in their simulation, as well as in their detection. We notice also that the polarization sign of *c*, *d*, and *e* peaks of Fig. 4 is well described by our surface band structure calculations, while the splitting of the *b* peak is barely visible within bulk states in Fig. 5. The Rashba splitting in the surface states of GaSe [Fig. 5(c)) is even less pronounced as compared with InSe, due to a smaller Ga atomic SOC, and can hardly be detected experimentally.

IV. CONCLUSIONS

We compare the experimental band structure of two promising *MX* compounds, ϵ-GaSe and ϵ-InSe. We show that the VBM is dominated by Se atoms, as proved by ARPES data of the top valence band, a comparable hole effective mass, and confirmed by calculations of orbital-projected bulk band structure. The predicted CBM, instead, is more influenced by the post-transition metals. Our description supports a major influence of the conduction band in affecting the electronic properties of related *MX* compounds. We also compare the valence band calculated within GGA-PBE, HSE06, and mBJ approaches with experimental data, showing limitations in describing band gap and valence band in depth. Finally, within the GGA-PBE approach, we describe Rashba-Bychkov spin splitting of surface states in ϵ-InSe and ϵ-GaSe. Overall, we show that the splitting of surface states is negligible, with the exception of selected states in ϵ-InSe emerging from the edge of bulk states. This picture is confirmed by our spin-ARPES measurements, showing the spin splitting of surface states in ϵ-InSe.

ACKNOWLEDGMENTS

The support by the Fundamental Research Program of the State Academies of Sciences (line of research III.23.2.9), and the project EUROFEL-ROADMAP ESFRI, are gratefully acknowledged. This work has been partly performed in the framework of the Nanoscience Foundry and Fine Analysis (NFFA—MIUR Italy Progetti Internazionali) facility. M. Castriota and F. Ciuchi are acknowledged for having performed, respectively, Raman and XRD characterization of GaSe and InSe samples. This work was supported by Saint Petersburg State University (Grant No. ID 51126254).

[1] Z. Ben Aziza, V. Zólyomi, H. Henck, D. Pierucci, M. G. Silly, J. Avila, S. J. Magorrian, J. Chaste, C. Chen, M. Yoon *et al.*, Phys. Rev. B **98**, 115405 (2018).
[2] A. Azizi, G. Antonius, E. Regan, R. Eskandari, S. Kahn, F. Wang, S. G. Louie, and A. Zettl, Nano Lett. **19**, 1782 (2019).
[3] P. Li and I. Appelbaum, Phys. Rev. B **92**, 195129 (2015).
[4] X. Li, M. W. Lin, A. A. Puretzky, J. C. Idrobo, C. Ma, M. Chi, M. Yoon, C. M. Rouleau, I. I. Kravchenko, D. B. Geohegan, and K. Xiao, Sci. Rep. **4**, 5497 (2014).
[5] D. V. Rybkovskiy, N. R. Arutyunyan, A. S. Orekhov, I. A. Gromchenko, I. V. Vorobiev, A. V. Osadchy, E. Yu. Salaev, T. K. Baykara, K. R. Allakhverdiev, and E. D. Obraztsova, Phys. Rev. B **84**, 085314 (2011).
[6] M. W. Chen, H. Kim, D. Ovchinnikov, A. Kuc, T. Heine, O. Renault, and A. Kis, npj 2D Mater. Appl. **2**, 2 (2018).
[7] D. J. Terry, V. Zólyomi, M. Hamer, A. V. Tyurnina, D. G. Hopkinson, A. M. Rakowski, S. J. Magorrian, N. Clark, Y. M. Andreev, O. Kazakova *et al.*, 2D Mater. **5**, 041009 (2018).
[8] D. A. Bandurin, A. V. Tyurnina, G. L. Yu, A. Mishchenko, V. Zólyomi, S. V. Morozov, R. K. Kumar, R. V. Gorbachev, Z. R. Kudrynskyi, S. Pezzini, Z. D. Kovalyuk *et al.*, Nat. Nanotechnol. **12**, 223 (2017).
[9] T. Wang, J. Li, Q. Zhao, Z. Yin, Y. Zhang, B. Chen, Y. Xie, and W. Jie, Materials **11**, 186 (2018).
[10] P. Hu, Z. Wen, L. Wang, P. Tan, and K. Xiao, ACS Nano **6**, 5988 (2012).
[11] Z. Ben Aziza, H. Henck, D. Pierucci, M. G. Silly, E. Lhuillier, G. Patriarche, F. Sirotti, M. Eddrief, and A. Ouerghi, ACS Nano **10**, 9679 (2016).
[12] H. Henck, D. Pierucci, J. Zribi, F. Bisti, E. Papalazarou, J.-C. Girard, J. Chaste, F. Bertran, P. Le Fèvre, F. Sirotti, L. Perfetti, C. Giorgetti, A. Shukla, J. E. Rault, and A. Ouerghi, Phys. Rev. Mater. **3**, 034004 (2019).
[13] Z. Ben Aziza, D. Pierucci, H. Henck, M. G. Silly, C. David, M. Yoon, F. Sirotti, K. Xiao, M. Eddrief, J.-C. Girard, and A. Ouerghi, Phys. Rev. B **96**, 035407 (2017).
[14] C. H. Lee, S. Krishnamoorthy, D. J. O'Hara, M. R. Brenner, J. M. Johnson, J. S. Jamison, R. C. Myers, R. K. Kawakami, J. Hwang, and S. Rajan, J. Appl. Phys. **121**, 094302 (2017).
[15] F. Yan, L. Zhao, A. Patanè, P. Hu, X. Wei, W. Luo, D. Zhang, Q. Lv, Q. Feng, C. Shen *et al.*, Nanotechnology **28**, 27LT01 (2017).
[16] W. Li, S. Poncé, and F. Giustino, Nano Lett. **19**, 1774 (2019).
[17] R. Longuinhos and J. Ribeiro-Soares, Phys. Chem. Chem. Phys. **18**, 25401 (2016).
[18] N. C. Fernelius, Prog. Cryst. Growth Charact. Mater. **28**, 275 (1994).
[19] J. Srour, M. Badawi, F. E. H. Hassan, and A. Postnikov, J. Chem. Phys. **149**, 054106 (2018).
[20] M. J. Hamer, J. Zultak, A. V. Tyurnina, V. Zólyomi, D. Terry, A. Barinov, A. Garner, J. Donoghue, A. P. Rooney, V. Kandyba *et al.*, ACS Nano **13**, 2136 (2019).
[21] T. Cao, Z. Li, and S. G. Louie, Phys. Rev. Lett. **114**, 236602 (2015).
[22] R. Fivaz and E. Mooser, Phys. Rev. **163**, 743 (1967).
[23] S. Sucharitakul, N. J. Goble, U. R. Kumar, R. Sankar, Z. A. Bogorad, F.-C. Chou, Y.-T. Chen, and X. P. A. Gao, Nano Lett. **15**, 3815 (2015).
[24] A. Sh. Abdinov, R. F. Babaeva, N. A. Ragimova, R. M. Rzaev, and S. I. Amirova, Inorg. Mater. **50**, 334 (2014).
[25] A. Segura, F. Pomer, A. Cantarero, W. Krause, and A. Chevy, Phys. Rev. B **29**, 5708 (1984).

[26] A. Chevy, A. Khun, and S. Martin, J. Cryst. Growth **38**, 118 (1977).
[27] I. Grimaldi, T. Gerace, M. M. Pipita, I. D. Perrotta, F. Ciuchi, H. Berger, M. Papagno, M. Castriota, and D. Pacilè, Solid State Commun. **311**, 113855 (2020).
[28] See Supplemental Material at http://link.aps.org/supplemental/10.1103/PhysRevMaterials.4.084603 for characterization by XRD of GaSe, additional ARPES and LEED measurements of InSe, and DFT calculations of both compounds.
[29] L. Quan, Y. Song, Y. Lin, G. Zhang, Y. Dai, Y. Wu, K. Jin, H. Ding, N. Pan, Y. Luo, and X. Wang, J. Mater. Chem. C **3**, 11129 (2015).
[30] Y. Ni, H. Wu, C. Huang, M. Mao, Z. Wang, and X. Cheng, J. Cryst. Growth **381**, 10 (2013).
[31] C. Bigi, P. K. Das, D. Benedetti, F. Salvador, D. Krizmancic, R. Sergo, A. Martin, G. Panaccione, G. Rossi, J. Fujii, and I. Vobornik, J. Synchrotron Radiat. **24**, 750 (2017).
[32] G. Kresse and J. Hafner, Phys. Rev. B **48**, 13115 (1993).
[33] G. Kresse and J. Furthmüller, Phys. Rev. B **54**, 11169 (1996).
[34] P. E. Blöchl, Phys. Rev. B **50**, 17953 (1994).
[35] G. Kresse and D. Joubert, Phys. Rev. B **59**, 1758 (1999).
[36] J. P. Perdew, K. Burke, and M. Ernzerhof, Phys. Rev. Lett. **77**, 3865 (1996).
[37] S. Grimme, J. Antony, S. Ehrlich, and H. Krieg, J. Chem. Phys. **132**, 154104 (2010).
[38] A. D. Becke and E. R. Johnson, J. Chem. Phys. **124**, 221101 (2006).
[39] F. Tran and P. Blaha, Phys. Rev. Lett. **102**, 226401 (2009).
[40] A. V. Krukau, O. A. Vydrov, A. F. Izmaylov, and G. E. Scuseria, J. Chem. Phys. **125**, 224106 (2006).